Chemical Engineering Journal 427 (2022) 131574

Contents lists available at ScienceDirect

Chemical Engineering Journal

journal homepage: www.elsevier.com/locate/cej

Accelerating discovery of COFs for CO_2 capture and H_2 purification using structurally guided computational screening

Gokhan Onder Aksu [a], Ilknur Erucar [b], Zeynep Pinar Haslak [a], Seda Keskin [a,*]

[a] Department of Chemical and Biological Engineering, Koc University, Rumelifeneri Yolu, Sariyer, 34450 Istanbul, Turkey
[b] Department of Natural and Mathematical Sciences, Faculty of Engineering, Ozyegin University, Cekmekoy, 34794 Istanbul, Turkey

ARTICLE INFO

Keywords:
Covalent organic framework (COF)
H_2 purification
CO_2 capture
Membrane
Molecular simulations
Density functional theory (DFT)

ABSTRACT

Screening of hypothetical covalent organic framework (hypoCOF) database enables to go beyond the current synthesized structures to design high-performance materials for CO_2 separation. In this work, we followed a structurally guided computational screening approach to find the most promising candidates of hypoCOF adsorbents and membranes for CO_2 capture and H_2 purification. Grand canonical Monte Carlo (GCMC) simulations were used to evaluate CO_2/H_2 separation performance of 3184 hypoCOFs for pressure-swing adsorption (PSA) and vacuum-swing adsorption (VSA) processes. CO_2/H_2 adsorption selectivities and CO_2 working capacities of hypoCOFs were calculated in the range of 6.13–742 (6.39–954) and 0.07–8.68 mol/kg (0.01–3.92 mol/kg), achieving higher values than those of experimentally synthesized COFs at PSA (VSA) conditions. Density functional theory (DFT) calculations revealed that the strength of hydrogen bonding between CO_2 and the functional group of linkers is an important factor for determining the CO_2 selectivity of hypoCOFs. The most predominant topologies and linker types were identified as bor and pts, linker91 (a triazine linker) and linker92 (a benzene linker) for the top-performing hypoCOF adsorbents, respectively. Molecular dynamics (MD) simulations of 794 hypoCOFs showed that they exceed the Robeson's upper bound by outperforming COF, zeolite, metal organic framework (MOF), and polymer membranes due to their high H_2/CO_2 selectivities, 2.66–6.14, and high H_2 permeabilities, 9×10^5–4.5×10^6 Barrer. Results of this work will be useful to guide the synthesis of novel materials by providing molecular-level insights into the structural features of hypothetical COFs to achieve superior CO_2 separation performance.

1. Introduction

Covalent organic frameworks (COFs) have emerged as exciting nanoporous materials due to their high performance in many industrial applications such as gas storage and separation [1–3]. COFs share similar structural properties with metal organic frameworks (MOFs), but different than MOFs, COFs are composed of covalently-bonded linkers containing only light elements (H, B, C, and O), which provide a lower mass density enabling much higher gravimetric gas uptakes compared to MOFs with similar surface areas [4]. Besides low density, COFs exhibit large surface areas and tuneable pore structures, enhancing their potential for gas storage and separation applications [5]. They consist of metal-free and electron rich monomers, making them environment friendly, cost-effective, and very resistant for different pH conditions. These properties enable them to be used in different sensing, photovoltaics, and catalytic applications [6–8]. The number of experimentally reported COFs is rapidly increasing, and molecular simulations play a critical role in assessing their gas storage and separation performances before experimental efforts [9–15].

High-throughput computational screening (HTCS) is an efficient approach for assessing the potential of several thousands of materials for various gas separations and guiding the experimental studies to the best materials [16–18]. To accelerate the HTCS studies of COFs, Computation-Ready Experimental COF (CoRE COF) [19–21] database consisting of 474 materials and Clean, Uniform, and Refined with Automatic Tracking from Experimental Database (CURATED COFs) [22,23] including 626 structurally optimized COFs were established. These two databases were used in HTCS for noble gas separations [19], storage of CH_4 [20] and H_2 [24], capture of iodine and methyl iodine [25], and CO_2 capture from syngas and flue gas mixtures [26,27]. For example, 298 CoRE COFs were screened for membrane-based CO_2/CH_4 separation, and results showed that functionalization with fluorine and

* Corresponding author.
E-mail address: skeskin@ku.edu.tr (S. Keskin).

https://doi.org/10.1016/j.cej.2021.131574
Received 26 May 2021; Received in revised form 8 July 2021; Accepted 29 July 2021
Available online 9 August 2021
1385-8947/© 2021 The Author(s). Published by Elsevier B.V. This is an open access article under the CC BY-NC-ND license (http://creativecommons.org/licenses/by-nc-nd/4.0/).

chlorine groups of 11 representative COFs increases gas separation performances of membranes [21]. Our group screened 295 CoRE COFs for adsorption-based and membrane-based CO_2/N_2 separation and COFs with narrow pores were found to outperform traditional adsorbents, such as zeolites and activated carbons, as having high CO_2 selectivities, and most COF membranes were shown to have similar CO_2 permeabilities compared to MOFs [26]. We recently screened 288 CoRE COFs and identified the top COF adsorbents having narrow pores (the largest cavity diameter (LCD) < 15 Å) and low porosities ($\phi < 0.75$) for selective CO_2 separation from H_2, and the top COF membranes with large pores (LCD > 20 Å) and high porosities ($\phi > 0.85$) for H_2 purification [27]. These studies focused on a limited number of experimentally synthesized COFs (~300 COFs); therefore, the knowledge obtained from structure-performance relationships of COFs that can lead to the design of new, high-performing materials has been limited to date.

To go beyond the experimental COF structures and to enlarge the materials space for developing statistically significant structure-performance relations, the hypothetical COF (computer-generated but not yet synthesized, hypoCOF) databases [24,28–31] were constructed. One of these hypoCOF databases, constructed by Zhong and coworkers [29], were screened for H_2 storage [24]. Results showed that COFs with topologies having the optimum pore sizes, ~10 Å, porosities, ~0.8, and simple linker units achieve high performances in terms of H_2 storage, excessing the Department of Energy (DOE) target. Another hypoCOF database, constructed by Smit and coworkers, consists of 69,840 structures generated by using *in silico* structure assembly process where various linkers are assembled in different topological nets [28]. They screened this database to compute CH_4 adsorption and found that almost 300 hypoCOFs exhibit high CH_4 deliverable capacities, competitive with the traditional adsorbents [28]. Screening hypoCOFs for CO_2/N_2 separation using parasitic energy revealed that almost 400 hypothetical materials have lower parasitic energy than that obtained from the traditional amine scrubbing process, suggesting that flue gas separation with hypoCOFs can be cost-efficient and more than 70 hypoCOFs performed better than the synthesized COFs [31]. Screening of this hypoCOF database to identify the best COF adsorbents and membranes with high potential for various gas separations will be very useful not only for guiding experiments towards synthesizing novel COFs but also for the conceptual understanding of the COF design.

In this study, we proposed an efficient and structurally directed computational screening approach to investigate both adsorption-based and membrane-based CO_2/H_2 separation performances of hypoCOFs. This pre-combustion separation is required to recover CO_2 from the syngas and with this approach, direct CO_2 emissions are prevented [32]. We previously showed that experimentally synthesized COFs with LCD < 15 Å and $\phi < 0.75$ are the best adsorbents, whereas the ones with LCD > 20 Å and $\phi > 0.85$ are the best membranes for CO_2/H_2 separation [27]. Motivated from these results of experimentally synthesized COFs, we developed a database refinement approach for hypoCOF materials space and screened 69,840 hypoCOFs. 3184 hypoCOFs having LCD < 15 Å and $\phi < 0.75$ were examined for adsorption-based CO_2/H_2 separation at pressure swing adsorption (PSA) and vacuum swing adsorption (VSA) conditions and 794 large-pored hypoCOFs were studied for membrane-based CO_2/H_2 separation. After calculating various adsorbent and membrane performance metrics, the top hypoCOF adsorbents and membranes were identified and compared with the experimentally synthesized COFs, MOFs, zeolites, and polymers. Both chemical descriptors of materials, such as heat of adsorption, topology, linker and bond type, dimensionality, and physical descriptors such as pore size, porosity, surface area were investigated to understand the common features of high-performing COF adsorbents and membranes. Density functional theory (DFT) calculations were performed on the selected hypoCOFs to reveal how chemical composition affects CO_2 and H_2 adsorption. Our results will provide molecular-level insights into the structural features of hypothetical COFs which have not been synthesized yet, but have higher potential than synthesized ones for CO_2/H_2 separation.

2. Computational details

We started with the hypoCOF database which consists of 69,840 structures [28]. HypoCOF structures were named as linkerA_linkerB_net_interp_#, where "A" and "B" denote the linkers and their respective linker terminations, "net" represents the topology and "#" shows the degree of interpenetration, if the structure is catenated [28]. The corresponding IUPAC (International Union of Pure and Applied Chemistry) [33] names of all linkers together with their three dimensional representations were available in the literature [28]. We computed the largest cavity diameter (LCD), accessible surface area (S_{acc}), density (ρ), and porosity (ϕ) values using Zeo++ software (version 0.3) [34]. Blind screening of all hypoCOFs is time-consuming due to the very large number of materials. Therefore, we performed a directed computational screening methodology as represented in Fig. 1, considering our recent results from the computational screening of 288 CoRE COFs (experimentally synthesized COFs) for adsorption-based and membrane-based CO_2/H_2 separation [27]. It was previously demonstrated that COF adsorbents with LCD < 15 Å and $\phi < 0.75$ and COF membranes with LCD > 20 Å and $\phi > 0.85$ outperform other CoRE COFs for CO_2/H_2 separation. Based on this outcome, two hypoCOF subsets, hypoCOF-A for adsorbents and hypoCOF-M for membranes, were constructed by filtering the materials considering their LCD and ϕ as shown in Fig. 1. For hypoCOF-A set, 3184 materials with LCD < 15 Å and $\phi <$ 0.75 were selected. For hypoCOF-M set, we selected 794 hypoCOFs with LCD and ϕ in the ranges of 50–85.7 Å and 0.90–0.99, respectively. Fig. 2 shows the LCD and ϕ distribution of hypoCOF-A and hypoCOF-M sets in addition to those of 288 CoRE COFs. We examined several chemical descriptors of COFs, including dimensionality (D), linker and bond types, and topological nets. HypoCOF-A set consists of 388 2D and 2796 3D materials with LCD < 15 Å and $\phi < 0.75$ whereas hypoCOF-M set includes 229 2D and 565 3D materials with LCD > 50 Å and $\phi > 0.9$. In hypoCOF-A (hypoCOF-M) set, there are 154 (30) different topological nets and 111 (95) linker types. Structural properties of all hypoCOFs studied in this work, together with their topology, linker, dimensionality information, and schematic representations of the linkers that we discussed throughout this study are provided in an excel file as Supplementary Information (SI).

The accuracy of our computational methodology was previously validated by comparing the experimental measurements with the results of molecular simulations for the single-component gas (CO_2, N_2, H_2, CH_4, C_2H_6, C_2H_4) and mixture (CO_2/H_2, CO_2/N_2, CH_4/H_2, CO_2/CH_4, CH_4/N_2) adsorption, and for the single-component gas (CO_2, N_2, H_2, CH_4, He) and mixture (CO_2/H_2, CO_2/CH_4) permeation in various types of MOFs and COFs [26,27,35–48]. In order to get CO_2 and H_2 uptakes for both hypoCOF-A and hypoCOF-M, Grand canonical Monte Carlo (GCMC) simulations were run using the RASPA software (version 2.0.36) [49]. The mole fractions of CO_2 and H_2 were set as 0.15 and 0.85 to mimic the industrial pre-combustion gas mixture [50]. We previously showed that MOFs can still achieve very high CO_2/H_2 selectivities in the presence of impurities ($CO_2/H_2/CO/CH_4/H_2O$), unless they have open metal sites or extra framework ions which can have strong interaction with H_2O [51]. Since there is no open metal sites or extra framework ions in the structures of hypoCOFs, impurities in the CO_2/H_2 mixture are not expected to dramatically affect our predicted separation performances for hypoCOFs. Following the literature [51–53], adsorption and desorption pressures were set at 10 (1) and 1 (0.1) bar for PSA (VSA) process, respectively, and molecular simulations were performed at 0.1, 1, and 10 bar and 298 K to acquire CO_2 and H_2 uptakes of hypoCOFs for PSA and VSA processes. Dispersion and electrostatic interactions were defined by using Lennard-Jones (LJ) and Coulomb potentials, respectively. H_2 was modeled by a single-site sphere with LJ 12–6 potential [54]. CO_2 was modeled as a linear, rigid molecule consisting of three sites with C-O bond length of 1.16 Å and point charges located at the

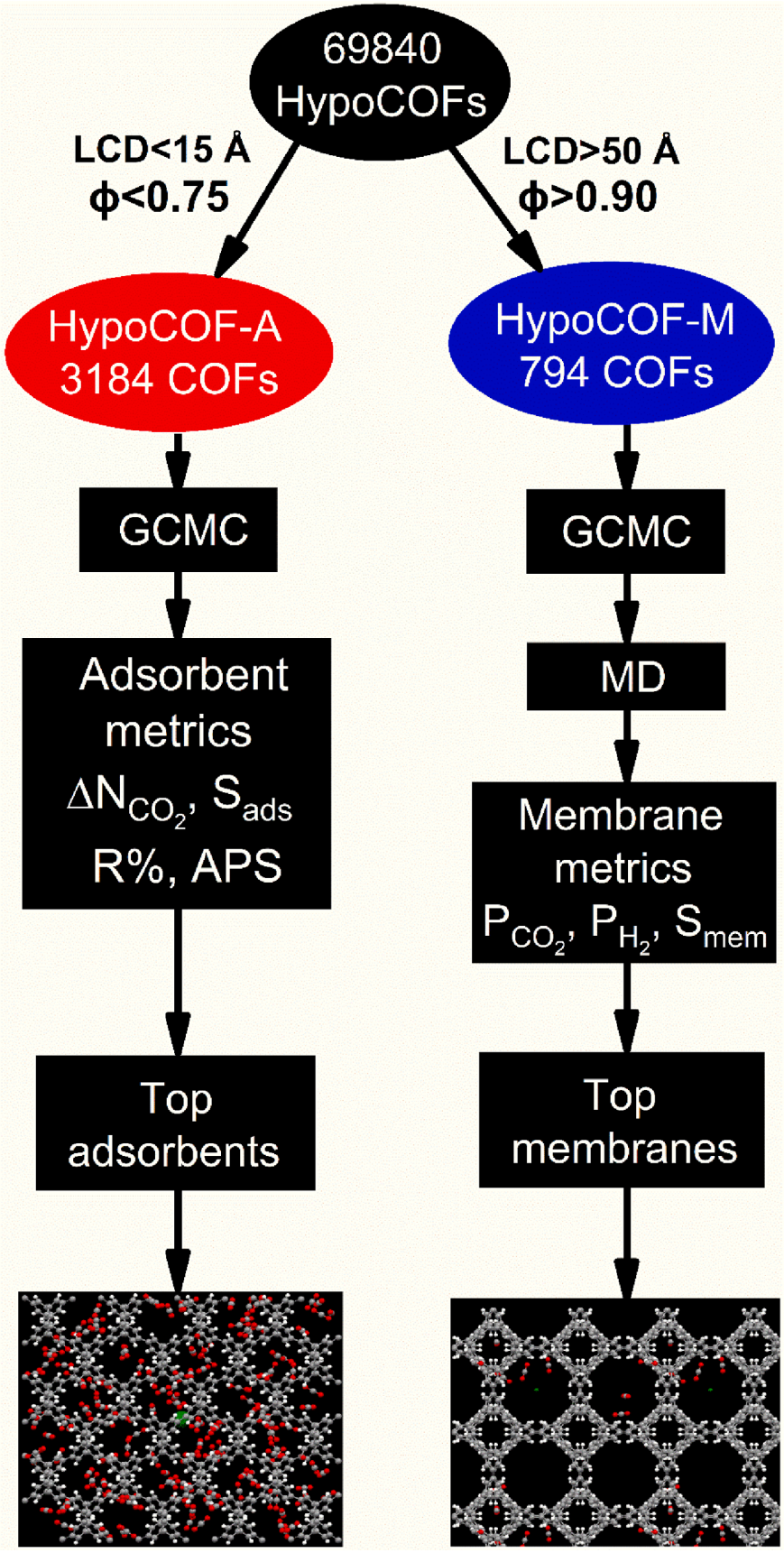

Fig. 1. Directed computational screening of hypoCOFs for adsorption-based and membrane-based CO_2/H_2 separation.

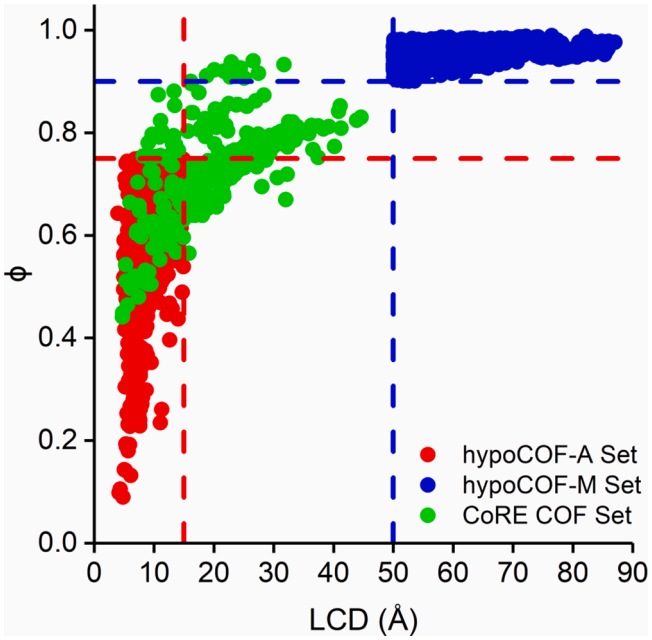

Fig. 2. Porosity and LCD comparison of hypoCOF-A and hypoCOF-M sets with CoRE COFs.

center of each site [55]. We used the Dreiding force field for LJ parameters of all hypoCOFs' atoms since in the previous computational studies on gas adsorption of hypoCOFs and COFs [20,22,24,26–28,31], results obtained from simulations with this force field were in good agreement with the isotherms of three different experimentally synthesized COFs, COF-5, COF-6, and COF-10 for adsorption of CO_2 and H_2 gases [27]. The charge equilibration method (Qeq), integrated into the RASPA, was used to assign point charges of hypoCOFs' atoms [56]. Electrostatic interactions between CO_2 molecules and hypoCOFs' atoms were defined using Ewald summation [57]. Lorentz-Berthelot mixing rules were used to estimate the interactions between non-identical atoms. Similar to our previous work [27], 10,000 cycles were used for initialization, and 20,000 cycles were used to take ensemble averages in GCMC simulations. Translation, regrow, reinsertion, swap, and identity exchange moves were defined for both CO_2 and H_2 molecules in binary mixture simulations, while rotation move was also added for only CO_2. Dimensions of the simulation box were expanded to at least 25.6 Å since the cut-off radius was set as 12.8 Å following the literature [28,31]. Peng-Robinson equation of state was applied to convert pressure to fugacity [49]. The isosteric heats of adsorption (Q_{st}) of CO_2 and H_2 were calculated using the fluctuation method [58]. The difference between the isosteric heats of adsorption of gases in materials, ΔQ_{st}, was computed by subtracting Q_{st,H_2} from Q_{st,CO_2} at 1 (0.1) and 10 (1) bar for PSA (VSA) process.

Molecular dynamics (MD) simulations in the canonical ensemble (NVT) were performed to calculate self-diffusivities (D_{self}) of CO_2 and H_2 in 794 hypoCOF-M materials. 10^6 cycles were used for initialization and equilibration, and then 5×10^6 cycles were used for production with the time step of 1 fs. The temperature was kept constant at 298 K by using the Nosé-Hoover thermostat [59]. The modified order-N algorithm, implemented in RASPA, was utilized to estimate the mean-square displacement (MSD) of gas molecules, and self-diffusivities were calculated using Einstein's relation [60]. The self-diffusivities obtained from MD simulations with predefined loadings were combined by the gas uptakes acquired from GCMC simulations at 10 bar, 298 K to compute the gas permeabilities through hypoCOFs. All hypoCOFs were assumed to be rigid to save computational time in MD simulations.

To analyze gas separation performances of hypoCOF adsorbents and membranes, GCMC and MD results were used to compute performance evaluation metrics as shown in Table S1. Adsorption selectivity (S_{ads}) was computed as the ratio of strongly adsorbed gas uptake (CO_2) to the weakly adsorbed gas uptake (H_2), normalized by the bulk gas compositions. Here, we note that hypoCOF-A set shown in Fig. 2 exhibits high adsorption selectivity (S_{ads}), whereas hypoCOF-M set shows low S_{ads} towards CO_2, indicating the importance of structurally guided computational screening, as we discuss in detail below. Working capacity (ΔN) shows how much CO_2 is captured at each adsorption cycle. Adsorbent performance score (APS), the multiplication of selectivity and working capacity [61], and percent regenerability (R%), the ratio of working capacity to the amount of adsorbed CO_2, was computed to identify the most promising adsorbents [62]. Gas permeability and selectivity are the two metrics used to evaluate the performance of membranes. Permeabilities (P_i) were computed by combining the results of GCMC and MD simulations, and membrane selectivity (S_{mem}) was computed by taking the ratio of the permeability of the more permeable gas and that of the less permeable gas.

We also performed density functional theory (DFT) calculations on the selected two hypoCOFs to understand the effect of linker types on CO_2 and H_2 adsorption. To reduce the computational cost, the pore parts of the COFs were represented by cluster models. The constrained environment of the COFs were mimicked by freezing the key atoms in cluster models, and the rest of the atoms were allowed to be fully optimized by using Becke-three-parameter-Lee-Yang-Parr (B3LYP) [63,64] functional with D2 correction scheme proposed by Grimme [65] and all-electron 6-31G* basis set using Gaussian09 program package [66]. The binding energies between the gases and COFs were calculated by using $\Delta E_{bind} = E_{COF+Gas} - (E_{COF} + E_{Gas}) + \delta^{BSSE}$ where $E_{COF+Gas}$ is the energy of the COF-gas complex, E_{COF} and E_{Gas} denote the COF and gas energies, and δ^{BSSE} is the basis set superposition error correction employed by Counter Poise approach. The partial atomic charges were derived from Natural Population Analysis (NPA) [67]. Cartesian coordinates of the optimized geometries for these hypoCOFs were provided in the excel file in SI.

3. Results and discussions

Both hypoCOF-A and hypoCOF-M sets were first evaluated for their CO_2/H_2 separation performances at PSA and VSA conditions. Fig. 3(a-b) depict the relationship between $S_{ads,CO_2/H_2}$ and ΔN_{CO_2} for a total of 3978 hypoCOFs composed of 3184 hypoCOF-A and 794 hypoCOF-M. HypoCOFs with low (<10 mol/kg), moderate (10–100 mol/kg), and high (>100 mol/kg) APSs are represented as black, blue, and red points, respectively. We observed that hypoCOFs in hypoCOF-A set with high $S_{ads,CO_2/H_2}$ tend to have low ΔN_{CO_2} and vice versa at PSA condition, as the correlation coefficient (R^2) was computed as 0.61. On the other hand, $S_{ads,CO_2/H_2}$ and ΔN_{CO_2} become more correlated at VSA condition, as R^2 increases to 0.84. In hypoCOF-A set, $S_{ads,CO_2/H_2}$ and ΔN_{CO_2} were computed as 6.1–742 (6.4–954) and 0.07–8.68 mol/kg (0.01–3.92 mol/kg), respectively, at PSA (VSA) condition. There are 993 (123) hypoCOF-A with high APSs (>100 mol/kg) and 2143 (1073) hypoCOF-A with moderate (10–100 mol/kg) APSs at PSA (VSA) condition. On the other hand, $S_{ads,CO_2/H_2}$ and ΔN_{CO_2} for hypoCOF-M set were computed to be much lower than those obtained for hypoCOF-A set, 1.34–5.09 (1.36–5.04) and 1.01–2.37 mol/kg (0.10–0.25 mol/kg), respectively, at PSA (VSA) condition. There is no hypoCOF-M with APS > 10 mol/kg for both processes and the highest APS for hypoCOF-M set is computed as 8.60 (0.92) mol/kg at PSA (VSA) condition.

This difference between the performance of hypoCOF-A and hypoCOF-M is due to the structural properties of materials that we selected in our directed screening methodology: Fig. S1(a-b) show how $S_{ads,CO_2/H_2}$ of hypoCOF-A, hypoCOF-M, and CoRE COFs change based on their LCD and ϕ at 1 and 10 bar. It is clear that all hypoCOFs with $S_{ads,CO_2/H_2} > 100$ belong to hypoCOF-A set and appear in the region of LCD < 15 Å and ϕ < 0.75 at both adsorption pressures. On the other hand, all materials in hypoCOF-M set have low $S_{ads,CO_2/H_2}$ (<25). This is

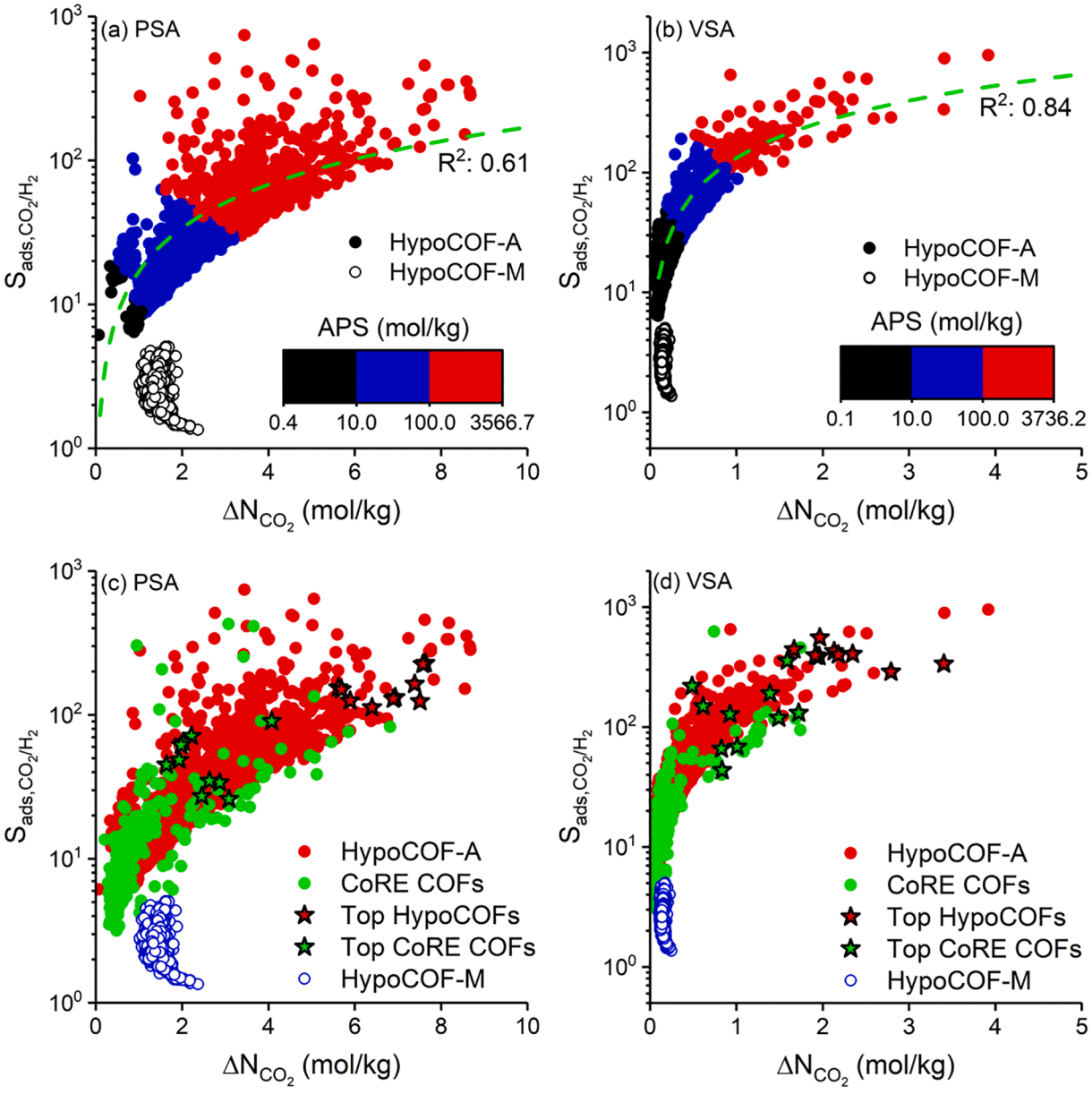

Fig. 3. Relations between $S_{ads,CO_2/H_2}$, ΔN_{CO_2}, and APS of hypoCOFs for CO_2/H_2:15/85 separation with correlation coefficients at (a) PSA and (b) VSA conditions. Black, blue, and red data show hypoCOFs with APS < 10 mol/kg, 10 mol/kg < APS < 100 mol/kg, and APS > 100 mol/kg, respectively. The green lines show the correlations according to the data of hypoCOF-A set. Comparison of hypoCOF-A and hypoCOF-M sets with the CoRE COFs was shown in (c-d).

due to the strong confinement of CO_2 molecules within the narrow pores of hypoCOF-A, leading to much higher $S_{ads,CO_2/H_2}$ compared to those obtained for larger pored hypoCOF-M. The relation between S_{acc} and $S_{ads,CO_2/H_2}$, shown in Fig. S1(c-d), also indicates that hypoCOFs with S_{acc} < 3500 m^2/g tend to have high adsorption selectivities (>100). Overall, hypoCOF-A set has higher potential in adsorption-based CO_2/H_2 separation than hypoCOF-M set at both PSA and VSA conditions as we expected, and these results show the importance of a directed computational screening approach to efficiently identify the high-performing adsorbents among thousands of candidates.

Since hypoCOF-A materials perform much better than hypoCOF-M materials at both PSA and VSA conditions, we considered only hypoCOF-A set to analyze the top adsorbents. For PSA and VSA processes, we identified the top 10 hypoCOF-A with the highest APSs among the materials exhibiting R% > 85%. High regenerability is one of the essential requirements in adsorption-based gas separation processes. Fig. S2(a-b) represent the relation between R% and APS of 3184 hypoCOFs at PSA and VSA conditions. 2726 (3113) hypoCOFs were computed to have R% > 85% at PSA (VSA) condition. For each process, the top 10 hypoCOF adsorbents with the highest APSs are shown with red points in Fig. S2(a-b) and listed in Tables S2–S3 with their structural features and performance metrics. CO_2 uptakes of the top 10 adsorbents were computed in the range of 6.52–8.93 (1.93–3.80) mol/kg at 10 (1) bar, 298 K. We observed that the best hypoCOF adsorbents at both conditions have small pore sizes (5 Å < LCD < 10 Å) and low porosities (0.40 < ϕ < 0.74), as shown in Tables S2–S3.

For PSA process, all the top 10 materials have LCD < 9 Å and ΔQ_{st} > 17 kJ/mol. For example, linker99_C_linker100_C_pts is the top performing hypoCOF at PSA condition. Since it has –OH functional groups and narrow pores (LCD:5.57 Å), CO_2 molecules are strongly confined (ΔQ_{st}:21.4 kJ/mol), leading to high $S_{ads,CO_2/H_2}$ (228). Linker104_C_linker92_C_hst is another top material with high $S_{ads,CO_2/H_2}$ (164) and ΔN_{CO_2} (7.39 mol/kg) for PSA process. This material also has narrow pores (LCD:6.50 Å) and low porosity (ϕ:0.69). Additionally, it

has –OH functional groups, which reside into the pores, favoring the adsorption of CO_2 molecules [3]. A similar trend is observed for VSA process as all of the top 10 materials have narrow pores (LCD < 7.5 Å) and their ΔQ_{st} are in the range of 9.90–21.9 kJ/mol. The best performing hypoCOF at VSA condition is linker92_C_linker92_C_bpi with $S_{ads,CO_2/H_2}$ of 336 and ΔN_{CO_2} of 3.40 mol/kg. It only consists of C and H atoms and has small pores (LCD:5.57 Å), enhancing adsorption selectivity. Another top material for VSA process is linker110_C_linker86_C_dia with a high $S_{ads,CO_2/H_2}$ (405) and the highest ΔQ_{st} (21.8 kJ/mol) among the top 10 hypoCOFs. It has -F and -S functional groups inside the pores favoring strong adsorption of CO_2 [21,68].

As we mentioned before, hypoCOFs were screened for adsorption-based CO_2/N_2 separation, and 72 top performers were identified according to metrics of parasitic energy and CO_2 working capacity [31]. When we checked the CO_2/H_2 separation performance of these 72 hypoCOFs, we found out that 7 (5) out of these 72 hypoCOFs are also

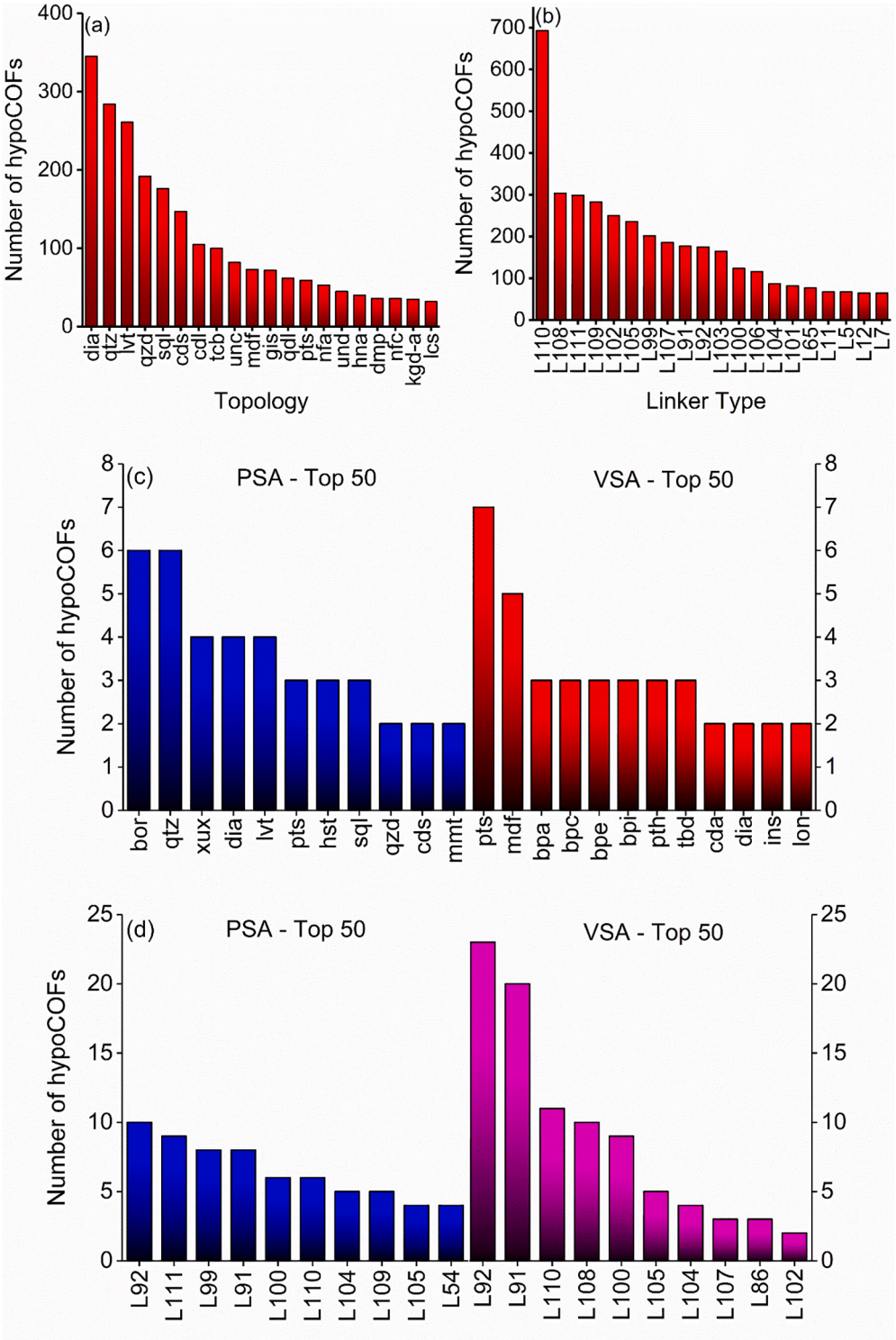

Fig. 4. Distributions of (a) the topological nets, (b) linker (L) types in hypoCOF-A set. The most common (c) topological nets and (d) linker types of the top-performing 50 hypoCOF-A at PSA and VSA conditions. The names of the linkers and their schematic representations are given in SI.

among in our top 10 hypoCOFs at VSA (PSA) condition, listed in Tables S2–S3. For example, linker92_C_linker92_utg, having a parasitic energy of 860 kJ and CO_2 working capacity of 0.11 kg CO_2/kg bed, was reported as a top adsorbent for CO_2/N_2 separation [31]. This hypoCOF is one of the top 10 adsorbents for CO_2/H_2 separation at VSA condition as listed in Table S3, having a $S_{ads,CO_2/H_2}$ of 388 and ΔN_{CO_2} of 1.96 mol/kg. These results prove that the potentials of hypoCOF adsorbents are needed to be unlocked for both syngas and flue gas separation.

To understand whether hypothetical COFs could perform better than experimentally synthesized COFs or not, we compared adsorption-based CO_2/H_2 separation performance of 3184 hypoCOFs in hypoCOF-A, 794 hypoCOFs in hypoCOF-M, and 288 experimentally synthesized CoRE COFs which were examined in our previous work in Fig. 3(c-d) [27]. $S_{ads,CO_2/H_2}$ and ΔN_{CO_2} of CoRE COFs were reported in the range of 2.38–428 (2.39–625) and 0.21–6.82 (0.02–1.74) mol/kg at PSA (VSA) condition. We observed that most hypoCOF-A materials have larger $S_{ads,CO_2/H_2}$ and ΔN_{CO_2} than CoRE COFs. On the other hand, hypoCOF-M set exhibits the lowest $S_{ads,CO_2/H_2}$ and ΔN_{CO_2} among these materials due to their larger pores compared to hypoCOF-A and CoRE COFs, as we discussed. We also highlighted the top 10 materials with the highest APSs and R% > 85% in Fig. 3(c-d). Results showed that hypoCOFs are computed to have APSs up to 3566 mol/kg (3736 mol/kg), almost six (two) times larger than the highest APS of the CoRE COFs at PSA (VSA) condition. The top 10 hypoCOF-A materials outperform the top 10 CoRE COFs at both conditions. For example, the best performing CoRE COF at PSA condition is TPE-COF-I [69], having APS of 368.2 mol/kg, $S_{ads,CO_2/H_2}$ of 90.4, ΔN_{CO_2} of 4.07 mol/kg [27]. 167 hypoCOF-A have APS > 368 mol/kg, which outperform TPE-COF-I. We performed the same analysis for VSA process, there are only 12 hypoCOF-A having APS > 566 mol/kg, the APS of the best performing experimental COF, NPN-1 [70]. Overall, results suggest that there are promising hypoCOFs, which have better performance than already-synthesized COFs for adsorption-based CO_2/H_2 separation.

Different linker types and topological nets were used for the construction of hypoCOFs. Therefore, we investigated how these structural and chemical differences affect the performance of adsorbents in terms of their CO_2/H_2 separation. Fig. 4(a-b) show the distributions of the most abundant 20 topologies and linker types in our hypoCOF-A set consisting of 3184 materials. The most abundant five topologies are dia, qtz, lvt, qzd, sql, and the most abundant linker types are linker102 (9,9′-spirobianthracene), linker108 (pyrene), linker109 (tetraphenylmethane), linker110 (adamantane) and linker111 (tetraphenylsilane) in all hypoCOF-A set. To understand the relationship between linker types, topologies, and performances of hypoCOFs, we extended our top material list to include the top 50 hypoCOF adsorbents and analyzed their topologies and linker types at PSA and VSA conditions in Fig. 4(c-d). The most predominant topologies are found as bor and qtz for PSA process. Qtz-hypoCOFs constitute the second largest group in hypoCOF-A set thus, its predominancy among the top materials is a natural result of the sampling. Bor-hypoCOFs also exhibit high adsorbent performance for CO_2/H_2 separation, although it is not one of the most abundant topologies in hypoCOF-A set. There are only 19 bor-hypoCOFs in the data set, and 6 of them are ranked in the top 50 materials due to their narrow pores (LCD < 8 Å). They provide very high CO_2 uptakes (5.03–6.28 mol/kg), resulting in higher $S_{ads,CO_2/H_2}$ (89.9–123) compared to $S_{ads,CO_2/H_2}$ of remaining bor-hypoCOFs (15.7–38.7) having larger pores (LCD:8.51–14.09 Å). On the other hand, pts- and mdf-hypoCOFs are the most predominant topologies for VSA process. The top materials identified for hypoCOF-A set at both PSA and VSA conditions have relatively smaller pores (LCD < 8 Å) compared to hypoCOFs having the same topological nets, resulting in high adsorption selectivity towards CO_2.

When we analyzed the performances of hypoCOFs for linker types, the most abundant linker is linker92 (benzene), a trigonal linker, at both PSA and VSA conditions among the top 50 hypoCOFs, as represented in Fig. 4(d). Linker91 (triazine) was shown to exhibit high CO_2 uptakes [71], and was found predominantly among the top 50 hypoCOFs at both conditions. We also observed that the linkers having –OH, –COOH, $–NH_2$, -S and -F functional groups, linker54 (3-oxo-3,4-dihydro quinoxaline-2-carboxylic acid), linker86 (2-(trifluoromethyl)-thiazolo [4,5-d]pyridazine), linker100 (2,2′-biphenol), linker104 (2,2′,4,4′-tetrahydroxybiphenyl), linker105 (4,4′-biphenol), and linker107 (4,4′-biphenyldiamine), are among the top 50 hypoCOFs for both processes since these functional groups generally increase CO_2 affinity, resulting in high $S_{ads,CO_2/H_2}$ [68]. For example, three top hypoCOFs having linker86, which is a linear linker containing strong electronegative functional groups -F and -S, were computed to have high $S_{ads,CO_2/H_2}$ (95–132) and high CO_2 uptakes (6.64–7.81 mol/kg). Top hypoCOFs containing linker100, linker104, and linker105, containing –OH groups, have also very high CO_2 uptakes (5.28–8.90 mol/kg), leading to very high $S_{ads,CO_2/H_2}$ (78–225) at 10 bar, 298 K. We investigated all possible hypoCOFs containing linker110, which is an adamantane-based tetragonal linker and the most common linker in our hypoCOF-A set. Both $S_{ads,CO_2/H_2}$ and ΔN_{CO_2} of these linker110-based hypoCOFs were found to vary in large ranges at PSA condition as shown in Fig. S3(a). This result indicates that although it is one of the predominant linkers among the top materials of both PSA and VSA processes, hypoCOFs having this linker are not guaranteed to be the top-performing adsorbents for CO_2/H_2 separation. For example, linker110_C_linker86_C_lcs was computed to have the highest $S_{ads,CO_2/H_2}$ (641) at PSA condition among the materials containing linker110 due to the presence of the functional groups (-F, and -S) in linker86 and small-pored (LCD:8.54 Å) structure. When the linker86 was changed with linker58 (pyrazine), which has no attached functional group, $S_{ads,CO_2/H_2}$ dramatically decreased to 16, although linker_110_C_linker58_C_ukd has a very similar pore size (LCD:8.50 Å) compared to the linker110_C_linker86_C_lcs. This example indicates that the linker functionalization has a significant effect on the performance of hypoCOFs. Another interesting example is linker110_C_linker86_C_uni which has the same linkers, but a lower $S_{ads,CO_2/H_2}$ (182) compared to its lcs-counterpart. Due to the topology, the former has a relatively large pore structure (LCD:11.79 Å), resulting in roughly four times lower $S_{ads,CO_2/H_2}$. We note that if hypoCOFs were refined considering the existence of certain functional groups, such as fluorine, at the beginning of our screening methodology, we would observe that COFs with very small pores outperform COFs with large pores in terms of CO_2/H_2 adsorption selectivities. Therefore, we can suggest that both structural and chemical properties determine the separation performance of hypoCOFs cooperatively. These results highlight the fact that both the chemical nature of the linker types and topologies should be considered to analyze the performance of the COF adsorbents for CO_2/H_2 separation.

To understand how topologies and linker types cooperatively affect the performance of hypoCOFs, we analyzed two cases: (i) materials having the same linkers but different topologies, (ii) materials having the same topology but different linkers. For case (i), we compared separation performances of hypoCOFs consisting of only linker92 with different topologies at VSA condition. linker92_C_linker92_C_bpi is a COF among the top 10 materials with $S_{ads,CO_2/H_2}$ and ΔN_{CO_2} of 336 and 3.40 mol/kg. The material, linker92_C_linker92_C_dmb, exhibits the poorest performance with $S_{ads,CO_2/H_2}$ and ΔN_{CO_2} of 44.1 and 0.51 mol/kg. Since the bpi-type COF has narrower pores (LCD:5.51 Å) than the dmb-type COF (LCD:8.34 Å), CO_2 molecules are strongly adsorbed inside the pores of the former, resulting in almost eight times higher CO_2 uptake. This large difference in CO_2 uptake of COFs leads to a large difference in their adsorption selectivities. For case (ii), we considered two lvt-type COFs, linker99_C_linker2_C_lvt_interp_3 and linker99_C_linker77_C_lvt_interp_3, in which both linker77 (4-methoxypyrimidine) and linker2 (phenol) were bonded to linker99 (biphenyl) through 2,5-carbon atoms. The former COF has the highest $S_{ads,CO_2/H_2}$ (155) and ΔN_{CO_2} (5.62 mol/kg) at PSA condition. When the second structural unit was changed from linker2 to linker77, $S_{ads,CO_2/H_2}$ and

ΔN_{CO_2} decreased to 66 and 2.70 mol/kg, respectively. To understand how these different linkers effect the gas adsorption in detail, we performed DFT calculations.

Two cluster models were generated for the representation of the pores of hypoCOFs as illustrated in Fig. 5. The adsorption sites for CO_2 and H_2 were determined by optimizing the gases inside the pores. As illustrated in Fig. 5(a-b), H_2 lies in close proximity to the biphenyl fragment and forms van der Waals interactions with the phenyl ring at a distance of 3.29 Å in linker99_C_linker2_C_lvt_interp_3 and of 3.62 Å in linker99_C_linker77_C_lvt_interp_3. Calculated binding energies were 1.06 and 0.35 kJ/mol meaning that adsorption of H_2 at biphenyl site is very similar in these hypoCOFs. As shown in Fig. S4, the partial atomic charges of the phenyl atoms with which H_2 molecules interact were calculated to be slightly different in both hypoCOFs. This points out that linker2 and linker77 do not alter the electronic configuration of the adsorption site. Thus, for this COF, changing linker2 to linker77 does not induce a major change in H_2 adsorption. Like H_2, CO_2 forms van der Waals interactions with phenyl fragments at a distance of 3.25 Å and 3.24 Å in linker99_C_linker2_C_lvt_interp_3 and linker99_C_linker77_C_lvt_interp_3, respectively, and interacts with the substituents on linker2 and linker77 as illustrated in Fig. 5(c-d). Calculated binding energies were 20.68 and 16.44 kJ/mol for the former and latter COF, respectively. Stronger hydrogen bond formed between CO_2 and –OH functional group on linker2 accounts for the stronger

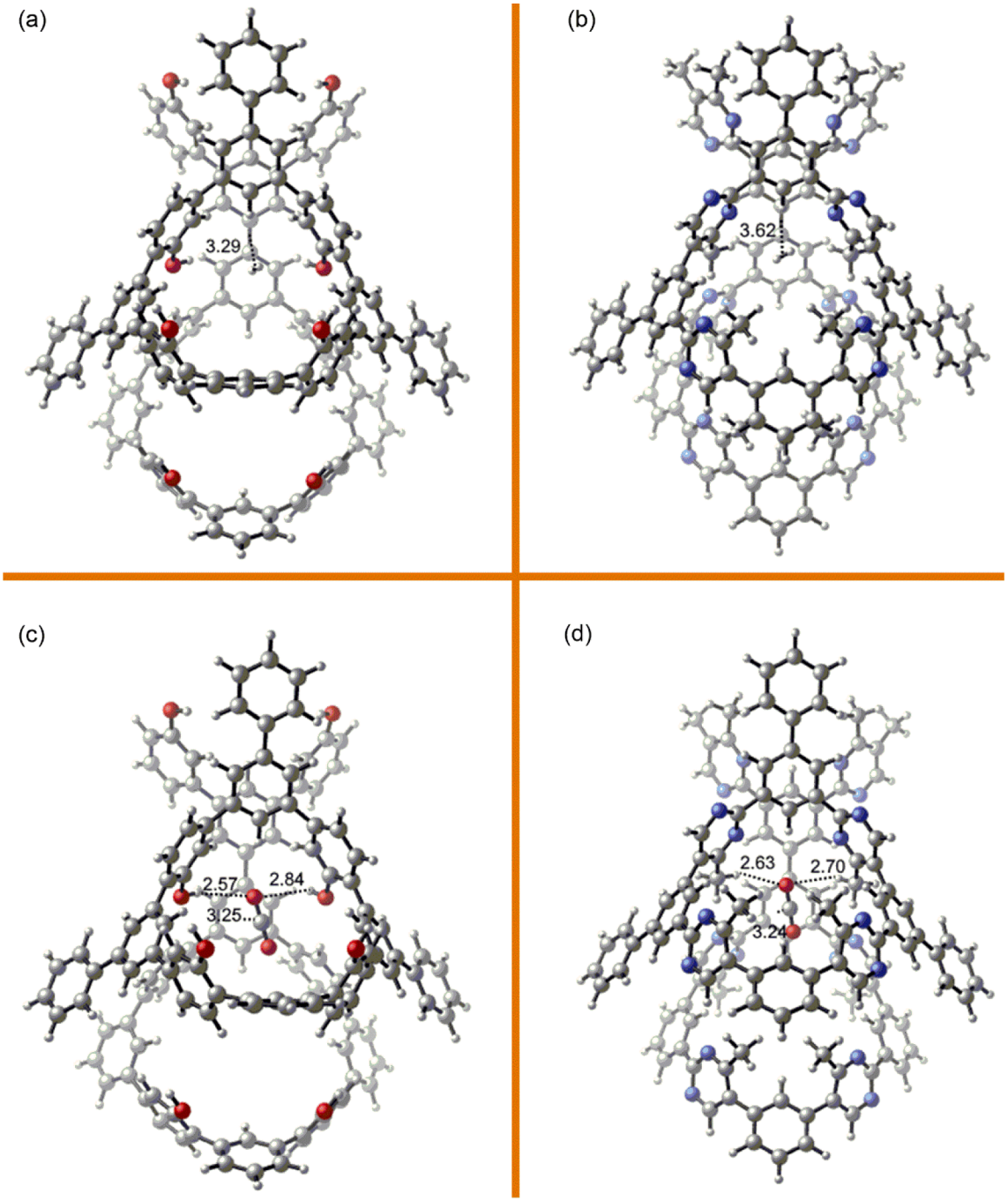

Fig. 5. 3D representations of the interactions of (a) H_2 with linker99_C_linker2_C_lvt_interp_3, (b) H_2 with linker99_C_linker77_C_lvt_interp_3, (c) CO_2 with linker99_C_linker2_C_lvt_interp_3, and (d) CO_2 with linker99_C_linker77_C_lvt_interp_3, calculated at B3LYP-D2/6-31G* level of theory. Bond distances are given in Å. Grey, white, red, and blue spheres represent C, H, O, and N atoms, respectively.

adsorption in linker99_C_linker2_C_lvt_interp_3 compared to the weaker adsorption in linker99_C_linker77_C_lvt_interp_3 due to the weaker hydrogen bond formed between CO_2 and $–CH_3$ functional group on linker77. O-H···O hydrogen bond plays more important role in stabilization of CO_2 molecules than C-H···O interaction since more electronegative oxygen atom withdraws the electrons from hydrogen in –OH, leaving the hydrogen electron deficient. On the other hand, carbon in $–CH_3$ is less electronegative than oxygen, withdrawing less electrons from hydrogens; as a result, hydrogens are less positive in $–CH_3$ compared to hydrogen of –OH. Electron rich oxygen of CO_2 makes stronger hydrogen bond with more positive hydrogen in –OH. Eventually, the higher CO_2 selectivity of linker99_C_linker2_C_lvt_interp_3 compared to linker99_C_linker77_C_lvt_interp_3 can be explained by the stronger adsorption of CO_2 due to the strong hydrogen bond formed between CO_2 and –OH functional group on linker2.

We also investigated the relation between dimensionalities of hypoCOFs and their adsorption-based separation performances in Fig. S5(a). 3D-hypoCOFs were computed to have higher $S_{ads,CO_2/H_2}$ and ΔN_{CO_2} than 2D-hypoCOFs at both PSA and VSA conditions. As shown in Fig. S5(b-c), 3D-hypoCOFs have denser structures and less S_{acc} compared to 2D-hypoCOFs. These dense 3D structures have stronger adsorption sites for CO_2 than layered structures of 2D-hypoCOFs. As an evidence, calculated ΔQ_{st} values of 3D-hypoCOFs, 7.8–27.2 kJ/mol, were found to be larger than those of 2D-hypoCOFs, 9.0–18.6 kJ/mol at PSA condition. Due to the presence of stronger adsorption sites, high $S_{ads,CO_2/H_2}$ (>100) were acquired for 3D-hypoCOFs, especially for frameworks with densities > 600 kg/m^3. The linker types used to synthesize hypoCOFs and interconnections of these linkers can describe the dimensionality and topological nets. For example, linker92_C_linker92_C_utg is a 3D-hypoCOF with $S_{ads,CO_2/H_2}$ of 288 and ΔN_{CO_2} of 2.79 mol/kg at VSA condition. If its second linker was changed to linker47 (phenazine), four 2D-hypoCOFs with different topologies, linker92_C_linker47_C_X (X:hcb, hnb, hna, tts-a), could be constructed and all of them have lower $S_{ads,CO_2/H_2}$ (29.1–54.1) and ΔN_{CO_2} (0.30–0.62 mol/kg) than the 3D-hypoCOF. 3D-hypoCOF can adsorb more CO_2 molecules (3.25 mol/kg) than those four 2D-hypoCOFs (0.33–0.69 mol/kg) due to its narrow pores (LCD:5.15 Å) and dense structure (693 kg/m^3).

HypoCOFs were classified according to their bond types and relations between $S_{ads,CO_2/H_2}$, ΔQ_{st}, LCD and ϕ were studied for five bond types used in the construction of hypoCOF database. In hypoCOF-A set, there are 2144 carbon–carbon (C–C), 475 imine, 262 amide, 211 amine, and 92 mixed bonded hypoCOFs. The general trend is that highly CO_2-selective hypoCOF adsorbents have LCD < 9 Å and ϕ < 0.65 for each bond group as shown in Fig. 6(a-e). We found that C–C bonded hypoCOFs show the highest performance as they achieve the largest $S_{ads,CO_2/H_2}$ (up to 742) and ΔN_{CO_2} (up to 8.68 mol/kg) at PSA condition as shown in Fig. 6(a) and Fig. S6. This group of hypoCOFs was computed to have the largest ΔQ_{st} values (up to 27.2 kJ/mol) at 10 bar. In Fig. 6(b-e), we observed that there is less number of imine (10), amide (7), amine (1), mixed (3) bonded hypoCOFs with $S_{ads,CO_2/H_2}$ > 100 compared to the number of C–C bonded hypoCOFs (125) . A possible explanation is that since C-N bond, found in amide, imine, amine and mixed bonded hypoCOFs, is longer than C–C bond [72], C–C bonded linkers in hypoCOFs tend to form small pores (LCD < 9 Å), enhancing CO_2 affinity, $S_{ads,CO_2/H_2}$ and ΔN_{CO_2}. C-N bonded hypoCOFs can suffer from low $S_{ads,CO_2/H_2}$ and ΔN_{CO_2} because of the large pores. It is important to note that majority of the COFs designed experimentally are imine based. We evaluated 475 imine-based COF adsorbents because of our directional screening methodology following the optimum structural limits (LCD < 15 Å and ϕ < 0.75). Our results showed that 10 imine-based hypoCOFs having smaller pores and low porosities (LCD < 7 Å and ϕ < 0.60) achieve high $S_{ads,CO_2/H_2}$ (>100).

Membrane-based separation technology using microporous materials is a key alternative for conventional methods for pre-combustion CO_2 capture [73]. For this reason, we finally investigated hypoCOF-M set for membrane-based CO_2/H_2 separation. In hypoCOF membranes, similar to other porous membranes, separation mechanism is based on adsorption-diffusion mechanism where gas molecules are first adsorbed on the COFs and then diffuse through the pores [74]. We specifically focused on H_2/CO_2 selectivities of membranes since H_2 molecules diffuse much faster than CO_2 due to the molecular mass difference [75,76]. Fig. 7(a) represents the relations between adsorption, diffusion, and membrane selectivities of 794 hypoCOF membranes computed at 10 bar, 298 K. $S_{ads,H_2/CO_2}$ of all hypoCOF membranes were computed less than unity (0.20–0.74) since hypoCOFs selectively adsorb CO_2 over H_2 as discussed above. Since H_2 molecules diffuse much faster than CO_2 inside the pores of hypoCOFs, all hypoCOFs have diffusion selectivities favoring H_2 ($S_{diff,H_2/CO_2}$:6.23–20). Diffusion selectivity dominates the adsorption selectivity for H_2 and makes all materials H_2-selective membranes. Fig. 7(b) compares hypoCOF membranes with CoRE COFs, MOFs, zeolites, and polymers. $S_{mem,H_2/CO_2}$ and P_{H_2} of hypoCOFs were computed in the ranges of 2.66–6.14 and 9×10^5-4.49×10^6 Barrer, respectively. Various zeolite membranes (NaX, NaY, TON, MFI, CHA, DDR, ERI, and TSC) were computed to have $S_{mem,H_2/CO_2}$ of 0.02–1.02, which indicates that they were almost non-selective for H_2, and P_{H_2} of 2.3×10^3-4.2×10^4 Barrer according to the results of binary mixture simulations at 10 bar and 300 K [77]. The most H_2-selective hypoCOF, linker103_CH_linker89_N_unh, exhibits six times larger H_2 selectivity ($S_{mem,H_2/CO_2}$:6.14) than TSC, which has the highest $S_{mem,H_2/CO_2}$ among zeolites (1.02). The performance of the best performing 20 MOF membranes were investigated at binary mixture condition at 1 bar, 298 K, and their $S_{mem,H_2/CO_2}$ and P_{H_2} were computed as 1.24–4.17 and 2.9×10^5-1.7×10^6 Barrer, respectively [51]. We observed that there are 496 hypoCOFs with $S_{mem,H_2/CO_2}$ > 4.17 and P_{H_2} > 1.6×10^6 Barrer, outperforming the top-performing MOF membrane, FOTNIN ($S_{mem,H_2/CO_2}$:4.17, P_{H_2}:1.6×10^6 Barrer). The most striking result is that all 794 hypoCOF membranes exceed the Robeson's upper bound [78], recommending that hypoCOF membranes that we studied outperform polymeric membranes. We also know that several zeolites and MOFs have high H_2/CO_2 selectivities (such as FAU:4.7–6.8 [79,80], NaX:4.6–12.5 [80,81], LTA:7.6 [82], ZIF-7:8.4–13.6 [83,84], and ZIF-8:4.6–7.3 [85,86]) due to their molecular sieving behavior. However, they suffer from low H_2 permeabilities (such as ZIF-7:6.7×10^2-3.4×10^3 Barrer; ZIF-8:2.8×10^3-2.2×10^4 Barrer, LTA:1.2×10^2 Barrer). In this work, since we considered hypoCOFs with large pores (LCD > 50 Å), they achieve H_2/CO_2 membrane selectivities as a maximum of 6.14, comparable to zeolites, ZIF-7 and ZIF-8, but they outdo both MOFs and zeolites in terms of H_2 permeabilities at least three orders (>10^6 Barrer). Overall, our results showed that many hypoCOF membranes perform much better than MOF, zeolite, and polymeric membranes for H_2/CO_2 separation under similar/the same operating conditions. Membrane performances of 288 CoRE COFs were examined in our previous work, and their $S_{mem,H_2/CO_2}$ and P_{H_2} were calculated in the ranges of 5.91×10^{-3}-4.74 and 599–1.5×10^6 Barrer at 10 bar, 298 K, respectively [27]. HypoCOFs also exhibit higher $S_{mem,H_2/CO_2}$ and P_{H_2} than CoRE COF membranes, as shown in Fig. 7(b). In order to get a better insight for this comparison, the relationship between $S_{mem,H_2/CO_2}$ and P_{H_2} of hypoCOF membranes and their comparison with the top 10 CoRE COF membranes was depicted in Fig. 7(c). 373 hypoCOFs (blue symbols) were computed to have very high permeabilities (P_{H_2} > 2×10^6 Barrer). We identified the top 10 hypoCOF membranes (red symbols) exhibiting the largest $S_{mem,H_2/CO_2}$ (5.85–6.14). Their structural features and computed performance metrics were provided in Table S4. We observed that the best hypoCOF membranes have large pore sizes (50 Å < LCD < 60 Å) and very high porosities (ϕ > 0.96). Most of hypoCOFs outperform the top 10 CoRE COF membranes ($S_{mem,H_2/CO_2}$:3.37–4.74, P_{H_2}:5.8×10^5-1.5×10^6 Barrer) in terms of both $S_{mem,H_2/CO_2}$ and P_{H_2}. For example, CCOF-2 [87] was reported as the best COF membrane for H_2/CO_2 separation, and its $S_{mem,H_2/CO_2}$ and P_{H_2} were computed as 4.74 and 1.5×10^6 Barrer,

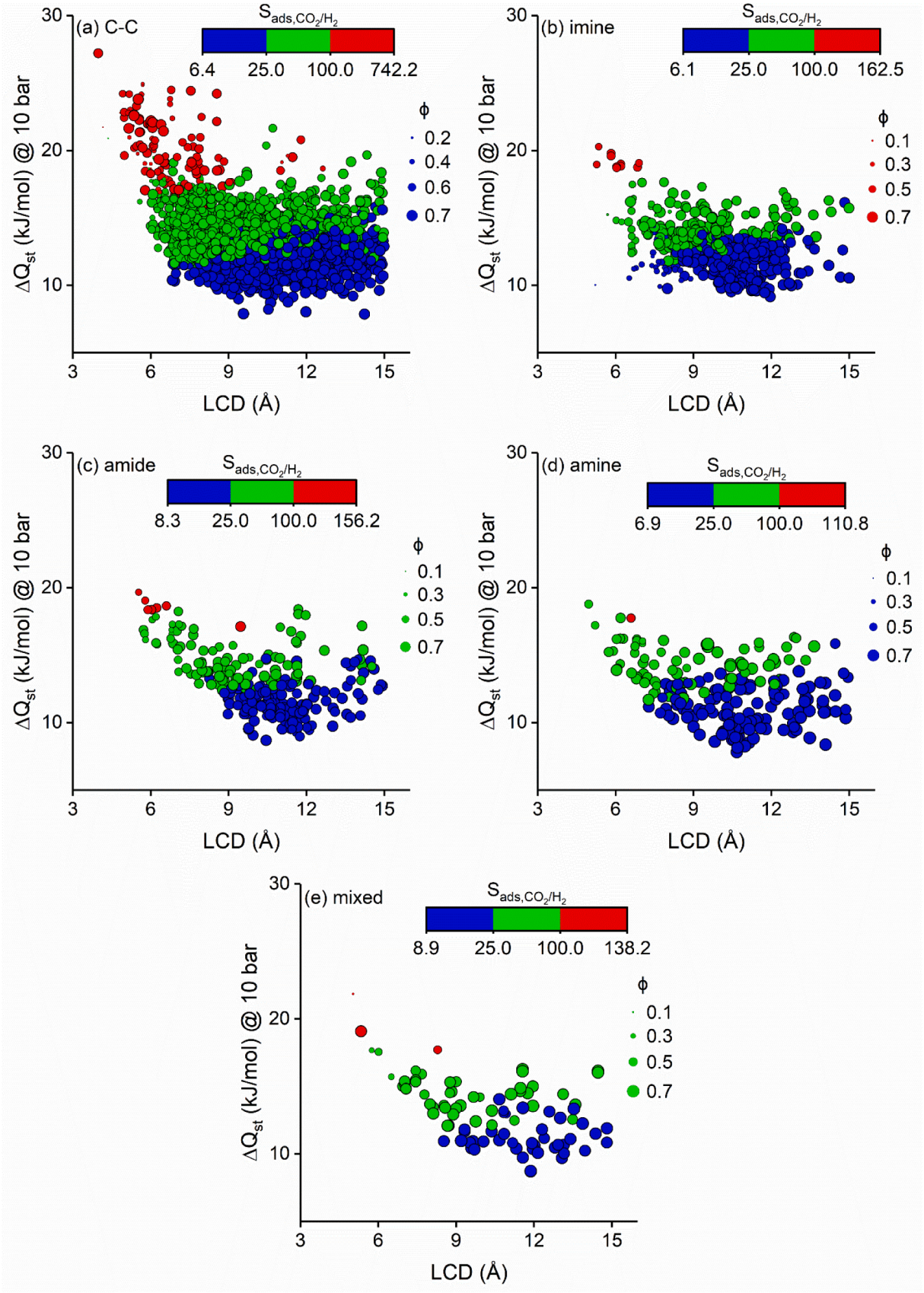

Fig. 6. Relations between $S_{ads,CO_2/H_2}$, ΔQ_{st} at 10 bar, LCD and ϕ of hypoCOF-A set for CO_2/H_2:15/85 separation at PSA condition for (a) C–C, (b) imine, (c) amide, (d) amine, and (e) mixed bonded hypoCOFs.

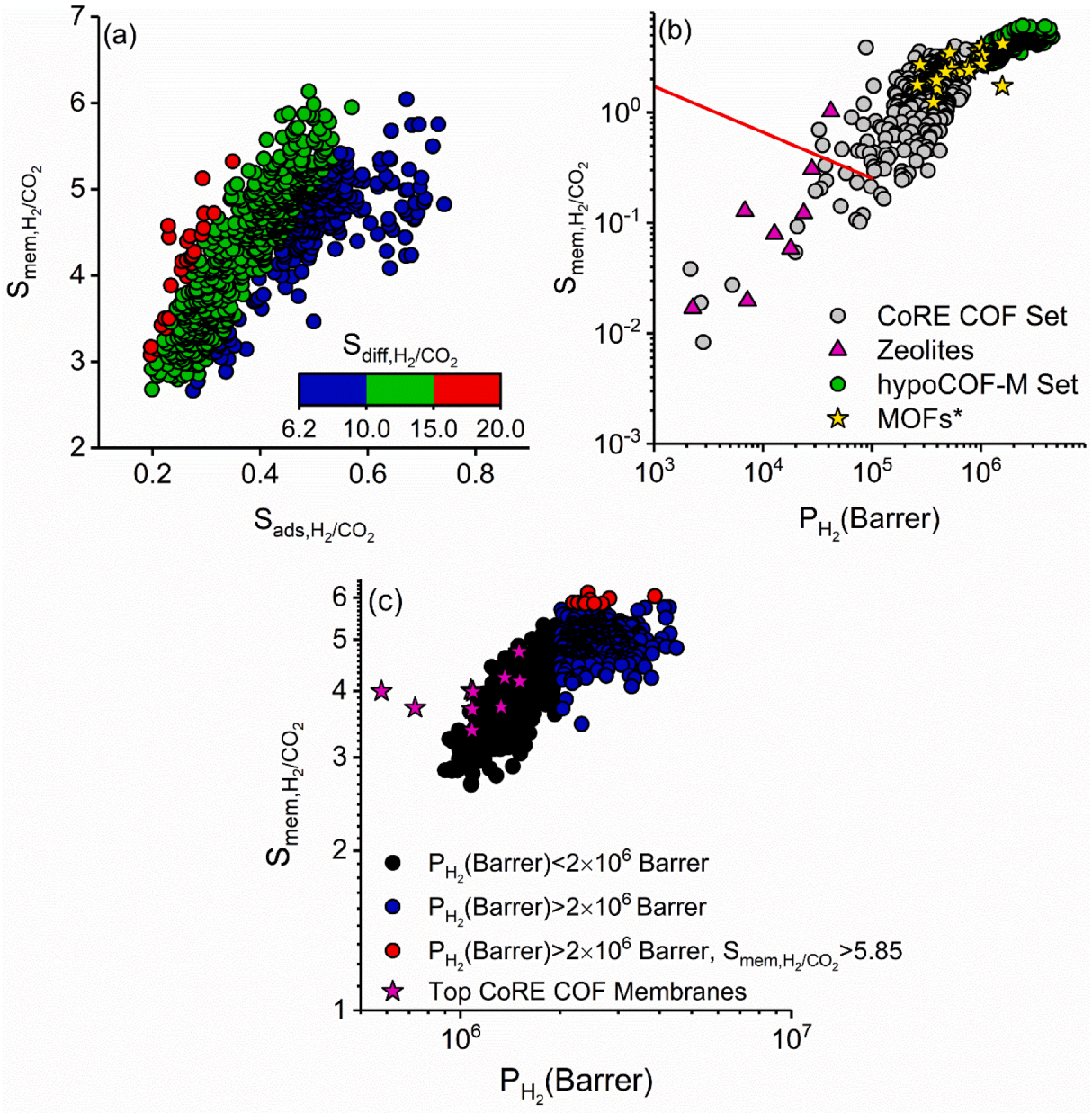

Fig. 7. (a) Comparison of adsorption, diffusion, and membrane selectivities of hypoCOF-M set calculated at 10 bar and 298 K. (b) Comparison of different membranes, zeolites, CoRE COFs, top 20 MOFs and polymers with hypoCOF-M set in terms of selectivity and H_2 permeability. (c) Relationship between membrane selectivity and H_2 permeability of hypoCOF-M set and comparison with the top CoRE COF membranes.

respectively [27]. In our hypoCOF-M set, there are 307 hypoCOF membranes offering $S_{mem,H_2/CO_2} > 4.74$ and all of them have $P_{H_2} > 1.5\times10^6$ Barrer. These results prove that there are hypoCOFs performing much better than already synthesized COFs for membrane-based H_2/CO_2 separation.

We note that since COFs are highly porous structures, experimentally synthesized COF membranes generally provide H_2/CO_2 selectivities as a maximum value of 14 [88,89]. Either functional groups were used within the pore environment or post synthesis treatment was applied to narrow down the pore sizes of COF membranes to enhance the selectivity [90]. For example, in a recent study, vertically aligned 2D COF membranes were fabricated and provided a very high H_2/CO_2 selectivity (31.6). It is indeed challenging to demonstrate the optimal adsorption and separation capacity of the experimental COF membranes since the synthesis methods, postsynthesis treatments and support layers can change their performance. We did not consider the factors related to the synthetic process, as our calculations are based on the gas permeabilities obtained for single COF crystals. We believe that potential hypoCOFs in this work can open new ways for the fabrication of highly selective membranes for H_2 purification.

The distributions of topologies and linker types for hypoCOF-M set and the best performing 50 hypoCOF membranes were shown in Fig. S7 (a-d). Among 794 hypoCOF-M, hca, rho and lta (linker103, linker94, and linker 102) are the most predominant topological nets (linker types). Comparing the results of hypoCOF-M set with those obtained for hypoCOF-A set, shown in Fig. 4(a-b), we found that only three linkers (linker91, linker92, and linker102) exhibit in both sets without any common topology. This result is expected since certain linkers and topologies are convenient for constructing small-pored or large-pored COFs. We observed that hypoCOFs with dia, qtz, and lvt topologies are mostly found in small-pored hypoCOFs (LCD < 15 Å), and large-pored hypoCOFs (LCD > 50 Å) mostly have hca, rho and lta

topologies as shown in Fig. 4(a) and Fig. S7(a), respectively. Fig. S8(a) represents the relationship between CO_2/H_2 adsorption selectivities and pore sizes of hypoCOFs with dia and hca, which are the most predominant topologies in small-pored hypoCOFs and large-pored hypoCOFs, respectively. When we consider all 3978 hypoCOFs evaluated in this work, there are 345 hypoCOFs with dia topology, and all of them have small pore sizes (LCD < 15 Å), resulting in high CO_2/H_2 adsorption selectivities up to 456. On the other hand, 186 hypoCOFs with hca topology exhibit large pore sizes (50–79.7 Å), leading to low CO_2/H_2 adsorption selectivities (2.46–5.09). We also observed the differences between the most predominant linkers among hypoCOF-A and hypoCOF-M sets, shown in Fig. 4(b) and Fig. S7(b). The reason is that small linkers, such as linker110, are convenient to construct small-pored hypoCOFs, whereas bulky and long linkers, such as linker94, are favorable for large-pored hypoCOFs. As shown in Fig. S8(b), there are 690 hypoCOFs containing linker110 among all 3978 hypoCOFs, and all of these hypoCOFs have small pores (LCD < 15 Å). On the other hand, linker94, one of the most abundant linkers among hypoCOF-M, contributed to 195 hypoCOFs and 176 of them have pores larger than 50 Å. These results show that different topologies and linkers lead to different structural properties which dramatically affect the CO_2/H_2 separation performance of hypoCOFs.

For top hypoCOF membranes, hypoCOFs with unh and sod topologies consist almost half of the top-performing 50 hypoCOF membranes, as shown in Fig. S7(c). Fig. S7(d) represents that linker103, linker94, and linker95 are the three most predominant linker types in top hypoCOF membranes. These linkers are very large and bulky due to four benzene rings; therefore, they are appropriate for constructing large-pored hypoCOFs, enhancing their diffusion selectivity towards H_2. Fig. S7(e) shows that 3D-hypoCOF membranes achieve higher separation performances than 2D-hypoCOF membranes as their $S_{mem,H_2/CO_2}$ and P_{H_2} were computed to be 3.47–6.14 and 1.2×10^6-4.3×10^6 Barrer, larger than those of 2D-hypoCOFs ($S_{mem,H_2/CO_2}$:2.66–4.40, P_{H_2}:9.0×10^5-2.0×10^6). To understand why 3D-hypoCOF membranes perform better than 2D-hypoCOFs, we compared their structural features with respect to S_{acc} and framework densities in Fig. S7(f). Results showed that 3D-hypoCOF membranes are less dense and have higher S_{acc} than 2D-hypoCOF membranes. Since less dense frameworks allow the adsorption of both gases, and H_2 diffuse faster than CO_2 within large pores, 3D-hypoCOF membranes exhibit high $S_{mem,H_2/CO_2}$ (>5), especially frameworks with densities less than 150 kg/m^3.

Overall, we found that hypoCOFs can be promising adsorbents and membranes, outperforming experimentally synthesized COFs, MOFs, polymers, and zeolites for precombustion CO_2 capture. We note that since this study is based on the identification of the most promising hypoCOFs, which are computer-generated and not experimentally synthesized structures, we have not considered the effect of orientation, packing and particle sizes of COF on their separation performance [28]. All these factors should be considered during the experimental fabrication of COF membranes [76]. Considering the good agreement between the computed powder X-ray diffraction (PXRD) patterns of some hypoCOFs with those obtained for their experimental analogues such as COF-300 and TAPB-PDA COF [28], we believe that our results will accelerate the synthesis of novel COFs with the joint efforts of experimental chemists and material scientists.

4. Conclusion

In this study, we screened 69,840 hypothetical COFs by using an efficient and structurally directed computational approach based on the structure-performance relations that we produced for experimentally synthesized COFs. Results showed that hypoCOF adsorbents outperform experimentally synthesized COFs in PSA (VSA) processes due to their high CO_2 selectivities, 6.13–742 (6.37–954), and large working capacities, 0.07–8.68 mol/kg (0.01–3.92 mol/kg). APSs of hypoCOFs were computed in the range of 0.43–3566 mol/kg and 0.05–3736 mol/kg, achieving almost six and two times larger upper limits than those of experimentally synthesized COFs at PSA and VSA conditions, respectively. DFT calculations on two hypoCOFs, which only differ in their linker fragments, showed that CO_2 and H_2 form van der Waals interactions with the linkers, whereas additional hydrogen bonds formed between CO_2 and linker substituents. The linker containing –OH substituents (linker2) form stronger hydrogen bonds with CO_2 than the linker with $–CH_3$ substituents attached (linker77), thus, higher $S_{ads,CO_2/H_2}$ is observed for the hypoCOF constructed from –OH functionalized linker. We then examined 794 hypoCOF membranes and showed that all hypoCOFs surpass the Robeson's upper bound due to their higher H_2 permeabilities (9×10^5-4.5×10^6 Barrer) and H_2/CO_2 selectivities (2.66–6.14) compared to those of polymer membranes. HypoCOFs outperformed experimentally synthesized COFs, zeolites, and MOFs as they achieve at least two times larger H_2/CO_2 membrane selectivities. Almost half of hypoCOF membranes was computed to have higher selectivity and permeability than the best experimental COF membrane, CCOF-2, reported in our previous work [27]. Results pointed out that hypoCOFs having bor- and pts-topologies with linker91 and linker92 tend to achieve very high adsorbent performances whereas unh- and sod-hypoCOFs with linker103 and linker94 were clear standouts among membranes. These results show that hypoCOFs are very promising adsorbents and membranes for CO_2 capture and H_2 purification. Considering the commercial availability of the linkers, synthesis of the promising hypoCOFs can lead to new, novel materials with high CO_2/H_2 separation performances.

Declaration of Competing Interest

The authors declare that they have no known competing financial interests or personal relationships that could have appeared to influence the work reported in this paper.

Acknowledgement

S.K. acknowledges ERC-2017-Starting Grant. This study has received funding from the European Research Council (ERC) under the European Union's Horizon 2020 research and innovation programme (ERC-2017-Starting Grant, grant agreement No 756489-COSMOS).

Appendix A. Supplementary data

Supplementary data to this article can be found online at https://doi.org/10.1016/j.cej.2021.131574.

References

[1] A.P. Cote, A.I. Benin, N.W. Ockwig, M. O'Keeffe, A.J. Matzger, O.M. Yaghi, Porous, crystalline, covalent organic frameworks, Science 310 (5751) (2005) 1166–1170.
[2] H. Furukawa, O.M. Yaghi, Storage of hydrogen, methane, and carbon dioxide in highly porous covalent organic frameworks for clean energy applications, J. Am. Chem. Soc. 131 (25) (2009) 8875–8883.
[3] Y. Zeng, R. Zou, Y. Zhao, Covalent organic frameworks for CO_2 capture, Adv. Mater. 28 (15) (2016) 2855–2873.
[4] H.M. El-Kaderi, J.R. Hunt, J.L. Mendoza-Cortes, A.P. Cote, R.E. Taylor, M. O'Keeffe, O.M. Yaghi, Designed synthesis of 3D covalent organic frameworks, Science 316 (5822) (2007) 268–272.
[5] S.-Y. Ding, W. Wang, Covalent organic frameworks (COFs): from design to applications, Chem. Soc. Rev. 42 (2) (2013) 548–568.
[6] S. Mondal, B. Mohanty, M. Nurhuda, S. Dalapati, R. Jana, M. Addicoat, A. Datta, B. K. Jena, A. Bhaumik, A thiadiazole-based covalent organic framework: a metal-free electrocatalyst toward oxygen evolution reaction, ACS Catal. 10 (10) (2020) 5623–5630.
[7] R. Gomes, A. Bhaumik, A new triazine functionalized luminescent covalent organic framework for nitroaromatic sensing and CO_2 Storage, RSC Adv. 6 (33) (2016) 28047–28054.
[8] S.K. Das, S. Mishra, K. Manna, U. Kayal, S. Mahapatra, K.D. Saha, S. Dalapati, G. Das, A.A. Mostafa, A. Bhaumik, A new triazine based π-conjugated mesoporous 2D covalent organic framework: its in vitro anticancer activities, ChemComm 54 (81) (2018) 11475–11478.

[9] G. Garberoglio, Computer simulation of the adsorption of light gases in covalent organic frameworks, Langmuir 23 (24) (2007) 12154–12158.
[10] R. Babarao, J. Jiang, Exceptionally high CO_2 storage in covalent-organic frameworks: atomistic simulation study, Energy Environ. Sci. 1 (1) (2008) 139–143.
[11] Q. Yang, C. Zhong, Molecular simulation study of the stepped behaviors of gas adsorption in two-dimensional covalent organic frameworks, Langmuir 25 (4) (2009) 2302–2308.
[12] M. Tong, Q. Yang, C. Zhong, Computational screening of covalent organic frameworks for CH_4/H_2, CO_2/H_2 and CO_2/CH_4 separations, Microporous Mesoporous Mater. 210 (2015) 142–148.
[13] S. Keskin, Adsorption, diffusion, and separation of CH_4/H_2 mixtures in covalent organic frameworks: molecular simulations and theoretical predictions, J. Phys. Chem. C 116 (2) (2012) 1772–1779.
[14] Y. Liu, D. Liu, Q. Yang, C. Zhong, J. Mi, Comparative study of separation performance of COFs and MOFs for $CH_4/CO_2/H_2$ Mixtures, Ind. Eng. Chem. Res. 49 (6) (2010) 2902–2906.
[15] M. Tong, Q. Yang, Y. Xiao, C. Zhong, Revealing the structure-property relationship of covalent organic frameworks for CO_2 capture from postcombustion gas: a multi-scale computational study, Phys. Chem. Chem. Phys. 16 (29) (2014) 15189–15198.
[16] M. Tong, Y. Lan, Q. Yang, C. Zhong, High-throughput computational screening and design of nanoporous materials for methane storage and carbon dioxide capture, Green Energy Environ. 3 (2) (2018) 107–119.
[17] H. Daglar, S. Keskin, Recent advances, opportunities, and challenges in high-throughput computational screening of MOFs for gas separations, Coord. Chem. Rev. 422 (2020), 213470.
[18] P.G. Boyd, Y. Lee, B. Smit, Computational development of the nanoporous materials genome, Nat. Rev. Mater. 2 (8) (2017) 1–15.
[19] M. Tong, Y. Lan, Q. Yang, C. Zhong, Exploring the structure-property relationships of covalent organic frameworks for noble gas separations, Chem. Eng. Sci. 168 (2017) 456–464.
[20] M. Tong, Y. Lan, Z. Qin, C. Zhong, Computation-ready, experimental covalent organic framework for methane delivery: screening and material design, J. Phys. Chem. C 122 (24) (2018) 13009–13016.
[21] T. Yan, Y. Lan, M. Tong, C. Zhong, Screening and design of covalent organic framework membranes for CO_2/CH_4 separation, ACS Sustain. Chem. Eng. 7 (1) (2019) 1220–1227.
[22] D. Ongari, A.V. Yakutovich, L. Talirz, B. Smit, Building a consistent and reproducible database for adsorption evaluation in covalent-organic frameworks, ACS Cent. Sci. 5 (10) (2019) 1663–1675.
[23] D. Ongari, L. Talirz, B. Smit, Too many materials and too many applications: an experimental problem waiting for a computational solution, ACS Cent. Sci. 6 (11) (2020) 1890–1900.
[24] M. Tong, W. Zhu, J. Li, Z. Long, S. Zhao, G. Chen, Y. Lan, An easy way to identify high performing covalent organic frameworks for hydrogen storage, ChemComm 56 (47) (2020) 6376–6379.
[25] Y. Lan, M. Tong, Q. Yang, C. Zhong, Computational screening of covalent organic frameworks for the capture of radioactive iodine and methyl iodide, CrystEngComm 19 (33) (2017) 4920–4926.
[26] O.F. Altundal, C. Altintas, S. Keskin, Can COFs replace MOFs in flue gas separation? high-throughput computational screening of COFs for CO_2/N_2 separation, J. Mater. Chem. A 8 (29) (2020) 14609–14623.
[27] G.O. Aksu, H. Daglar, C. Altintas, S. Keskin, Computational selection of high-performing covalent organic frameworks for adsorption and membrane-based CO_2/H_2 separation, J. Phys. Chem. C 124 (41) (2020) 22577–22590.
[28] R. Mercado, R.-S. Fu, A.V. Yakutovich, L. Talirz, M. Haranczyk, B. Smit, In silico design of 2D and 3D covalent organic frameworks for methane storage applications, Chem. Mater. 30 (15) (2018) 5069–5086.
[29] Y. Lan, X. Han, M. Tong, H. Huang, Q. Yang, D. Liu, X. Zhao, C. Zhong, Materials genomics methods for high-throughput construction of COFs and targeted synthesis, Nat. Commun. 9 (1) (2018) 1–10.
[30] R.L. Martin, C.M. Simon, B. Medasani, D.K. Britt, B. Smit, M. Haranczyk, In silico design of three-dimensional porous covalent organic frameworks via known synthesis routes and commercially available species, J. Phys. Chem. C 118 (41) (2014) 23790–23802.
[31] K.S. Deeg, D. Damasceno Borges, D. Ongari, N. Rampal, L. Talirz, A.V. Yakutovich, J.M. Huck, B. Smit, In silico discovery of covalent organic frameworks for carbon capture, ACS Appl. Mater. Interfaces 12 (19) (2020) 21559–21568.
[32] C. Antonini, K. Treyer, A. Streb, M. van der Spek, C. Bauer, M. Mazzotti, Hydrogen Production from Natural Gas and Biomethane with Carbon Capture and Storage–A Techno-Environmental Analysis, Sustain. Energy Fuels 4 (6) (2020) 2967–2986.
[33] L. Ettre, Nomenclature for chromatography (IUPAC Recommendations 1993), Pure Appl. Chem. 65 (4) (1993) 819–872.
[34] T.F. Willems, C.H. Rycroft, M. Kazi, J.C. Meza, M. Haranczyk, Algorithms and tools for high-throughput geometry-based analysis of crystalline porous materials, Microporous Mesoporous Mater. 149 (1) (2012) 134–141.
[35] Z. Sumer, S. Keskin, Molecular simulations of MOF adsorbents and membranes for noble gas separations, Chem. Eng. Sci. 164 (2017) 108–121.
[36] Z. Sumer, S. Keskin, Adsorption- and membrane-based CH_4/N_2 separation performances of MOFs, Ind. Eng. Chem. Res. 56 (30) (2017) 8713–8722.
[37] C. Altintas, S. Keskin, Molecular simulations of MOF membranes for separation of ethane/ethene and ethane/methane mixtures, RSC Adv. 7 (82) (2017) 52283–52295.
[38] O. Kadioglu, S. Keskin, Efficient separation of helium from methane using MOF membranes, Sep. Purif. Technol. 191 (2018) 192–199.
[39] C. Altintas, I. Erucar, S. Keskin, High-throughput computational screening of the metal organic framework database for CH_4/H_2 separations, ACS Appl. Mater. Interfaces 10 (4) (2018) 3668–3679.
[40] C. Altintas, G. Avci, H. Daglar, E. Gulcay, I. Erucar, S. Keskin, Computer simulations of 4240 MOF membranes for H_2/CH_4 separations: insights into structure-performance relations, J. Mater. Chem. A 6 (14) (2018) 5836–5847.
[41] H. Daglar, S. Keskin, Computational screening of metal-organic frameworks for membrane-based $CO_2/N_2/H_2O$ separations: best materials for flue gas separation, J. Phys. Chem. C 122 (30) (2018) 17347–17357.
[42] C. Altintas, S. Keskin, Molecular simulations of MOF membranes and performance predictions of MOF/polymer mixed matrix membranes for CO_2/CH_4 separations, ACS Sustain. Chem. Eng. 7 (2) (2019) 2739–2750.
[43] C. Altintas, G. Avci, H. Daglar, A.N.V. Azar, I. Erucar, S. Velioglu, S. Keskin, An extensive comparative analysis of two MOF databases: high-throughput screening of computation-ready MOFs for CH_4 and H_2 adsorption, J. Mater. Chem. A 7 (16) (2019) 9593–9608.
[44] A.N.V. Azar, S. Velioglu, S. Keskin, Large-scale computational screening of metal organic framework (MOF) membranes and MOF-based polymer membranes for H_2/N_2 separations, ACS Sustain. Chem. Eng. 7 (10) (2019) 9525–9536.
[45] H. Daglar, S. Keskin, High-throughput screening of metal organic frameworks as fillers in mixed matrix membranes for flue gas separation, Adv. Theory Simul. 2 (11) (2019) 1900109, https://doi.org/10.1002/adts.v2.1110.1002/adts.201900109.
[46] C. Altintas, S. Keskin, Role of partial charge assignment methods in high-throughput screening of MOF adsorbents and membranes for CO_2/CH_4 separation, Mol. Syst. Des. Eng. 5 (2) (2020) 532–543.
[47] G. Avci, I. Erucar, S. Keskin, Do New MOFs Perform Better for CO_2 Capture and H_2 Purification? Computational Screening of the Updated MOF Database, ACS Appl. Mater. Interfaces 12 (37) (2020) 41567–41579.
[48] H. Daglar, H.C. Gulbalkan, G. Avci, G.O. Aksu, O.F. Altundal, C. Altintas, I. Erucar, S. Keskin, Effect of Metal-Organic Framework (MOF) Database Selection on the Assessment of Gas Storage and Separation Potentials of MOFs, Angew. Chem. Int. Ed. 133 (14) (2021) 7907–7916.
[49] D. Dubbeldam, S. Calero, D.E. Ellis, R.Q. Snurr, RASPA: molecular simulation software for adsorption and diffusion in flexible nanoporous materials, Mol. Simul. 42 (2) (2016) 81–101.
[50] S. Lin, M. Harada, Y. Suzuki, H. Hatano, Hydrogen production from coal by separating carbon dioxide during gasification, Fuel 81 (16) (2002) 2079–2085.
[51] G. Avci, S. Velioglu, S. Keskin, High-throughput screening of MOF adsorbents and membranes for H_2 purification and CO_2 capture, ACS Appl. Mater. Interfaces 10 (39) (2018) 33693–33706.
[52] J.R. Hufton, S. Mayorga, S. Sircar, Sorption-enhanced reaction process for hydrogen production, AIChE J. 45 (2) (1999) 248–256.
[53] M. Fischer, Porous aluminophosphates as adsorbents for the separation of CO_2/CH_4 and CH_4/N_2 mixtures–a monte carlo simulation study, Sustain. Energy Fuels 2 (8) (2018) 1749–1763.
[54] V. Buch, Path integral simulations of mixed Para-D_2 and Ortho-D_2 clusters: the orientational effects, J. Chem. Phys. 100 (10) (1994) 7610–7629.
[55] J.J. Potoff, J.I. Siepmann, Vapor-liquid equilibria of mixtures containing alkanes, carbon dioxide, and nitrogen, AICHE J. 47 (7) (2001) 1676–1682.
[56] C.E. Wilmer, R.Q. Snurr, Towards rapid computational screening of metal-organic frameworks for carbon dioxide capture: calculation of framework charges via charge equilibration, Chem. Eng. J. 171 (3) (2011) 775–781.
[57] P. Ewald, Evaluation of optical and electrostatic lattice potentials, Ann. Phys. 64 (1921) 253–287.
[58] P. Nicholson, D. Nicholson, W. Nicholson, N.G. Parsonage, Computer Simulation and The Statistical Mechanics of Adsorption, Academic Press, London; New York, 1982.
[59] D.J. Evans, B.L. Holian, The nose–hoover thermostat, J. Chem. Phys. 83 (8) (1985) 4069–4074.
[60] A. Einstein, Investigations on the Theory of the Brownian Movement, Courier Corporation, New York, 1956.
[61] Y.G. Chung, D.A. Gómez-Gualdrón, P. Li, K.T. Leperi, P. Deria, H. Zhang, N. A. Vermeulen, J.F. Stoddart, F. You, J.T. Hupp, O.K. Farha, R.Q. Snurr, In silico discovery of metal-organic frameworks for precombustion CO_2 capture using a genetic algorithm, Sci. Adv. 2 (10) (2016) e1600909, https://doi.org/10.1126/sciadv.1600909.
[62] Y.-S. Bae, R.Q. Snurr, Development and evaluation of porous materials for carbon dioxide separation and capture, Angew. Chem. Int. Ed. 50 (49) (2011) 11586–11596.
[63] A.D. Becke, Density-functional thermochemistry. III. The Role of Exact Exchange, J. Chem. Phys. 98 (7) (1993) 5648–5652.
[64] C. Lee, W. Yang, R.G. Parr, Development of the colle-salvetti correlation-energy formula into a functional of the electron density, Phys. Rev. B 37 (2) (1988) 785–789.
[65] S. Grimme, J. Antony, S. Ehrlich, H. Krieg, A Consistent and Accurate Ab Initio Parametrization of Density Functional Dispersion Correction (DFT-D) for The 94 Elements H-Pu, J. Chem. Phys. 132 (15) (2010) 154104–154118.
[66] M.J. Frisch, G.W. Trucks, H.B. Schlegel, G.E. Scuseria, M.A. Robb, J.R. Cheeseman, G. Scalmani, V. Barone, G.A. Petersson, H. Nakatsuji, X. Li, M. Caricato, A.V. Marenich, J. Bloino, B.G. Janesko, R. Gomperts, B. Mennucci, H.P. Hratchian, J.V. Ortiz, A.F. Izmaylov, J.L. Sonnenberg, Williams, F. Ding, F. Lipparini, F. Egidi, J. Goings, B. Peng, A. Petrone, T. Henderson, D. Ranasinghe, V.G. Zakrzewski, J. Gao, N. Rega, G. Zheng, W. Liang, M. Hada, M. Ehara, K. Toyota, R. Fukuda, J. Hasegawa, M. Ishida, T. Nakajima, Y. Honda, O. Kitao, H. Nakai, T. Vreven, K. Throssell, J.A. Montgomery Jr., J.E. Peralta, F. Ogliaro, M.J. Bearpark, J.J. Heyd,

E.N. Brothers, K.N. Kudin, V.N. Staroverov, T.A. Keith, R. Kobayashi, J. Normand, K. Raghavachari, A.P. Rendell, J.C. Burant, S.S. Iyengar, J. Tomasi, M. Cossi, J.M. Millam, M. Klene, C. Adamo, R. Cammi, J.W. Ochterski, R.L. Martin, K. Morokuma, O. Farkas, J.B. Foresman, D.J. Fox, Gaussian 09 Rev. E.01, Wallingford, CT, 2009.

[67] A.E. Reed, R.B. Weinstock, F. Weinhold, Natural population analysis, J. Chem. Phys. 83 (2) (1985) 735–746.

[68] F. Yuan, Z. Yang, X. Zhang, C. Tong, G. Gahungu, W. Li, J. Zhang, Judicious design functionalized 3D-COF to enhance CO_2 adsorption and separation, J. Comput. Chem. 42 (13) (2021) 888–896.

[69] Q. Gao, X. Li, G.-H. Ning, H.-S. Xu, C. Liu, B. Tian, W. Tang, K.P. Loh, Covalent organic framework with frustrated bonding network for enhanced carbon dioxide storage, Chem. Mater. 30 (5) (2018) 1762–1768.

[70] D. Beaudoin, T. Maris, J.D. Wuest, Constructing monocrystalline covalent organic networks by polymerization, Nat. Chem. 5 (10) (2013) 830–834.

[71] P. Katekomol, J. Roeser, M. Bojdys, J. Weber, A. Thomas, Covalent triazine frameworks prepared from 1, 3, 5-tricyanobenzene, Chem. Mater. 25 (9) (2013) 1542–1548.

[72] J. Huheey, T. Cottrell, The strengths of chemical bonds, Butterworths Publications Ltd. (1958).

[73] N. Prasetya, N.F. Himma, P.D. Sutrisna, I.G. Wenten, B.P. Ladewig, A review on emerging organic-containing microporous material membranes for carbon capture and separation, Chem. Eng. J. 391 (2020), 123575.

[74] Q. Qian, P.A. Asinger, M.J. Lee, G. Han, K. Mizrahi Rodriguez, S. Lin, F. M. Benedetti, A.X. Wu, W.S. Chi, Z.P. Smith, MOF-Based Membranes for Gas Separations, Chem. Rev. 120 (16) (2020) 8161–8266.

[75] R.W. Baker, Membrane Technology and Applications, 2nd ed., John Wiley & Sons, Chichester, 2004.

[76] S. Yuan, X. Li, J. Zhu, G. Zhang, P. Van Puyvelde, B. Van der Bruggen, Covalent Organic Frameworks for Membrane Separation, Chem. Soc. Rev. 48 (10) (2019) 2665–2681.

[77] R. Krishna, J.M. van Baten, In Silico Screening of Metal-Organic Frameworks in Separation Applications, Phys. Chem. Chem. Phys. 13 (22) (2011) 10593–10616.

[78] L.M. Robeson, The Upper Bound Revisited, J. Membr. Sci. 320 (1-2) (2008) 390–400.

[79] A. Huang, N. Wang, J. Caro, Seeding-Free Synthesis of Dense Zeolite FAU Membranes on 3-Aminopropyltriethoxysilane-Functionalized Alumina Supports, J. Membr. Sci. 389 (2012) 272–279.

[80] P. Roy, N. Das, Synthesis of NaX Zeolite-Graphite Amine Fiber Composite Membrane: Role Of Graphite Amine in Membrane Formation for H_2/CO_2 separation, Appl. Surf. Sci. 480 (2019) 934–944.

[81] X. Yin, G. Zhu, Z. Wang, N. Yue, S. Qiu, Zeolite P/NaX Composite Membrane for Gas Separation, Microporous Mesoporous Mater. 105 (1-2) (2007) 156–162.

[82] A. Huang, F. Liang, F. Steinbach, T.M. Gesing, J.R. Caro, Neutral and Cation-Free LTA-Type Aluminophosphate ($AlPO_4$) Molecular Sieve Membrane with High Hydrogen Permselectivity, J. Am. Chem. Soc. 132 (7) (2010) 2140–2141.

[83] Y. Li, F. Liang, H. Bux, W. Yang, J. Caro, Zeolitic Imidazolate Framework ZIF-7 Based Molecular Sieve Membrane for Hydrogen Separation, J. Membr. Sci. 354 (1-2) (2010) 48–54.

[84] S. Qiu, M. Xue, G. Zhu, Metal-Organic Framework Membranes: From Synthesis to Separation Application, Chem. Soc. Rev. 43 (16) (2014) 6116–6140.

[85] L. Fan, M. Xue, Z. Kang, H. Li, S. Qiu, Electrospinning Technology Applied in Zeolitic Imidazolate Framework Membrane Synthesis, J. Mater. Chem. 22 (48) (2012) 25272–25276.

[86] X. Zhang, Y. Liu, S. Li, L. Kong, H. Liu, Y. Li, W. Han, K.L. Yeung, W. Zhu, W. Yang, New Membrane Architecture with High Performance: ZIF-8 Membrane Supported on Vertically Aligned ZnO Nanorods for Gas Permeation and Separation, Chem. Mater. 26 (5) (2014) 1975–1981.

[87] X. Wang, X. Han, J. Zhang, X. Wu, Y. Liu, Y. Cui, Homochiral 2D Porous Covalent Organic Frameworks for Heterogeneous Asymmetric Catalysis, J. Am. Chem. Soc. 138 (38) (2016) 12332–12335.

[88] H. Lu, C. Wang, J. Chen, R. Ge, W. Leng, B. Dong, J. Huang, Y. Gao, A Novel 3D Covalent Organic Framework Membrane Grown on A Porous α-Al_2O_3 Substrate Under Solvothermal Conditions, ChemComm 51 (85) (2015) 15562–15565.

[89] H. Fan, A. Mundstock, A. Feldhoff, A. Knebel, J. Gu, H. Meng, J. Caro, Covalent Organic Framework-Covalent Organic Framework Bilayer Membranes for Highly Selective Gas Separation, J. Am. Chem. Soc. 140 (32) (2018) 10094–10098.

[90] H. Fan, M. Peng, I. Strauss, A. Mundstock, H. Meng, J. Caro, High-Flux Vertically Aligned 2D Covalent Organic Framework Membrane With Enhanced Hydrogen Separation, J. Am. Chem. Soc. 142 (15) (2020) 6872–6877.